Iron losses minimization case applied for the optimization of an embedded hybrid claw pole alternator

K. Moufida* N. Chaker** A. Helmi** N. Rafik*

* Laboratory of Electronics and Information Technologies, University of Sfax, ENIS, Sfax, Tunisia

** Laboratory of Advanced Electronic Systems and Sustainable Energy, University of Sfax, ENET'Com, Sfax, Tunisia

***Abstract*--This paper aims to present a performance constrained optimization process of an embedded hybrid claw pole alternator for automotive applications where the excitation winding is transferred to the stator side using a non-linear reluctant network modeling. Proposed procedure is based on a Sequential Quadratic Programming (SQP) coupled to a magnetic equivalent circuit of the studied alternator targeting the minimization if iron losses. It has been found that the efficiency of the alternator could be improved especially at high speed rate.**

***Index Terms*—Optimization, embedded alternator, claw pole, hybrid excitation, magnetic equivalent circuit, iron losses.**

1. NOMENCLATURE

μ_0	: air permeability
μ_r	: relative permeability
L	: flux path average length
Su	: section area
ϕ	: magnetic flux tube crossing the section S
$H(B)$	: magnetic field
F	: loop m.m.f vector
R	: diagonal matrix of reluctances
S	: topological matrix
Ψ	: loop fluxes vector
D	: rotor diameter
L_r	: rotor length
v	: tangential speed of the rotor
L_{spire_moy}	: average length of a turn
N_{spires}	: number of turns per phase
$S_{fil\ stator}$	: wire section
a	: number of parallel wiring channels
δ	: parameterization of the coupling (δ=1 if triangular coupling, δ=0 if star coupling)
I_f	: alternator's field current
R_f	: resistance of the inductor
K_h	: the hysteresis current's constant
K_{cf}	: the eddy current's constant
α	: the Steinmetz constant
f	: frequency of the magnetic flux waveform;
B	: flux density
B_m	: peak of the sinusoidal flux density.
B_{co_m}	: maximum induction in magnetic collector
B_{cul_m}	: maximum induction in laminated parts
B_{cm_m}	: maximum induction in massive parts
K_s	: characteristic factor of the material
K_c	: Carter coefficient
$pas_{dentaire}$	: teeth pitch
b	: notch opening
B_e	: medium induction in the air gap
ρ	: electric resistivity of material
P_u	: electrical output power

2. INTRODUCTION

Embedded alternator provides the conversion of engine's mechanical energy into electrical energy through the stored magnetic energy in the air-gap [1]. The electromechanical energy conversion is achieved in order to transmit electrical energy to the battery and to all electric embedded receptors on the vehicle. Because of the increasing insist for on-board power, a continuous development of automotive alternators has been marked during the last years as to efficiency and power density is necessary [2],[3]. The claw pole alternator (CPA) is the conventional source of electrical energy in automotive applications.

In fact, CPA is characterized by the hetero-polar structure of its rotor offering the integration a high pole pair number in a reduced volume, leading so to an interesting generation capabilities [4]. In a previous paper [5], we proposed two modified structures of an automotive claw pole alternator, a Simple Excited Automotive Alternator (SE2A) and a Hybrid Excited Automotive Alternator (HE2A), where DC-excitation winding is transferred from rotor side to stator one as illustrated in Fig. 1.

These configurations are compared using an analytical tool based on reluctant modeling validated experimentally. In HE2A, the gain of Barium ferrites permanent magnets integration between claws emanates from the combination of the high-energy density of permanent magnets with the commonly controllability (Fig. 2). Through the investigation of hybridization effect, it has been found that it leads to the increase of alternator generation capabilities gathered to a fully controllable flux density [5].

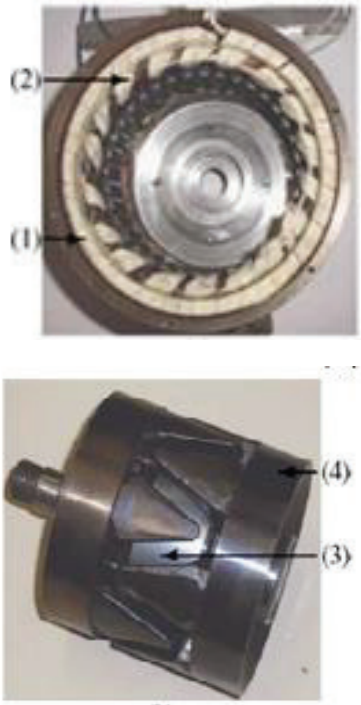

Fig. 1. Built prototype of the SE2A. Legend: (a) Sator of the SE2A, (b) rotor of the SE2A, (1) half of the stator DC-excitation ring winding, (2) armature en winding, (3) non-magnetic core, (4) magnetic collector.

Fig. 2. Rotor of HE2A with magnets inserted between claws

The idea of the present work consists on the improvement of the HE2A performance through the optimization of its topology. To do so, based on flux linkage between stator and rotor magnetic circuits, a reluctant network of the studied alternator is provided. Then, no-load and load operation performances are carried out in order to analyze the energetic state of the claw pole alternator. The final part concerns the optimization of the device topology considering iron losses minimization case.

2. MAGNETIC CIRCUIT MODEL OF THE HE2A

In a first step, a description of the flux paths through the magnetic circuit of the HE2A, Fig. 3, is necessary in order to build alternator magnetic equivalent circuit. They are of two kinds: useful (3D) and useless (2D):

- ✓ The 3D flux happens under each two poles and crosses both stator and rotor magnetic circuits. It is devoted to the generation of the emf in alternator's armature.
- ✓ The 2D flux is treated as leakage fluxes caused by homopolar linkage between rotor and stator.

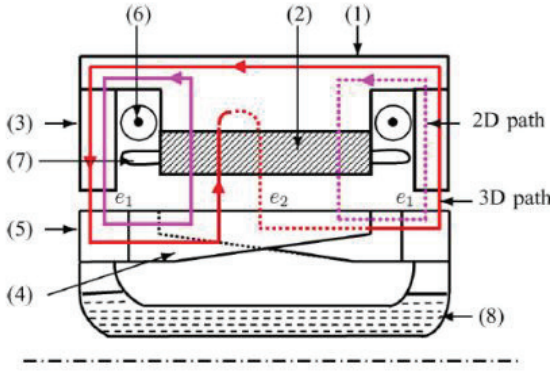

Fig. 3. Flux paths through the magnetic circuit of the HE2A. Legend: (1) to (5) same as in Fig. 1, (6): half of the stator DC-excitation winding, (7): armature end-winding, (8): non-magnetic core holding the two magnetic rings.

The magnetic equivalent circuit (MEC) can offer a compromise between short calculation time with adequate precision [6]. The MEC approach consists on the decomposition of alternator geometry into flux tubes based on the flux linkage through magnetic parts. These flux tubes correspond to reluctances, MMF sources and permanent magnets sources. The establishment of reluctant model of an actuator is based mainly on geometry dimensions, material characteristics, and winding distributions. To define different components, the Ohm magnetic law is applied following the analogy between electric circuits and magnetic ones.

The proposed HE2A network taking into account the armature magnetic reaction is illustrated in Fig. 4.

In the case of linear material, the reluctance is expressed as follows:

$$R = \frac{L}{\mu_0 \mu_r Su} \tag{1}$$

However, in the case of saturated material, reluctance is calculated using equation (2):

$$R = \frac{L}{\phi} H\left(\frac{\phi}{Su}\right) \tag{2}$$

Due to the non-linear behavior of the alternator materials [7], the Newthon-Raphson numerical algorithm is adopted to resolve established model and calculate needed values of flux crossing alternator's armature [8]. Indeed, the number of equations to be resolved is same as independent loops in considered circuit. In the case of non-saturated magnetic circuit, the obtained system is given by equation (3). However, when materials are saturated, the inversion of matrix (SRS^T) is no longer possible. Then the MEC system is transformed to equation (4) and resolution procedure is completed when all elements of vector C turn to be null, [5].

$$\Psi = SRS^T{}^{-1} F \tag{3}$$

$$C = F - SRS^T \Psi \tag{4}$$

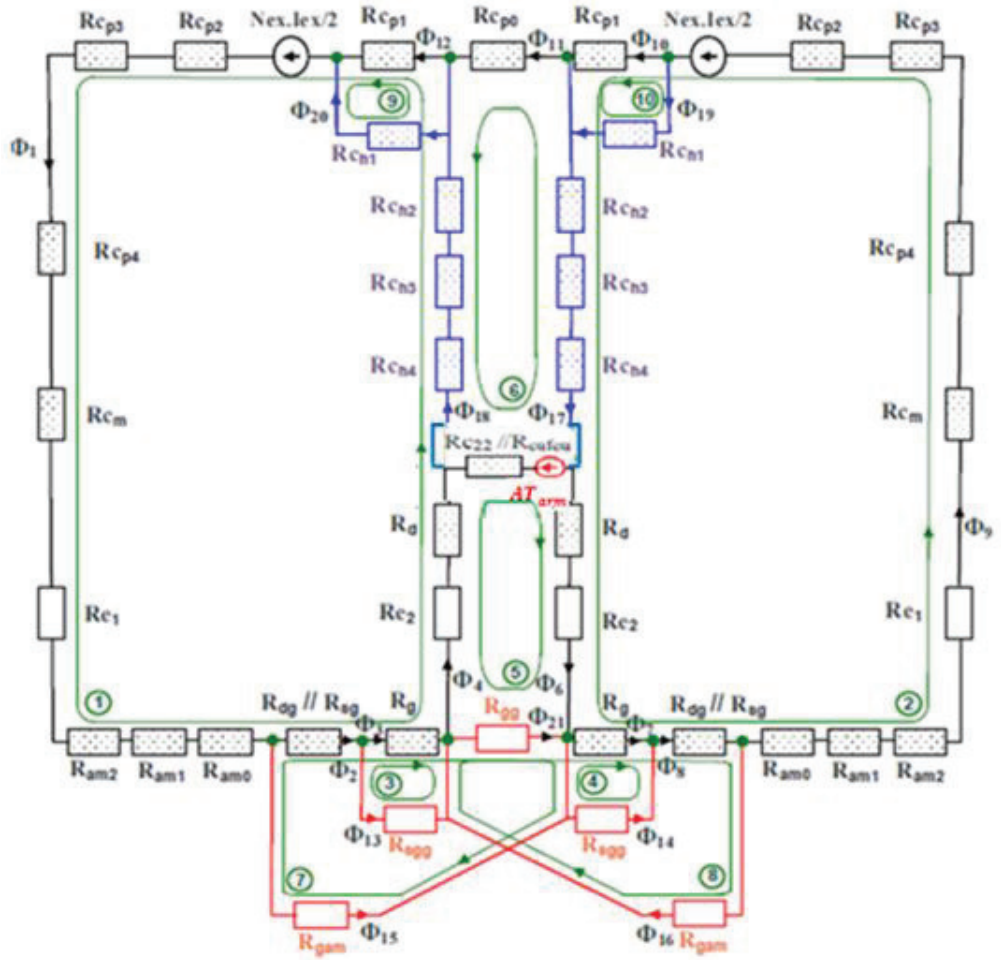

Fig. 4. HE2A reluctance network within the d-axis accounting for the armature magnetic reaction and the saturation.

3.Losses And Efficiency of the HE2A

Losses in the Hybrid Excited Automotive Alternator (HE2A) are grouped into mechanical losses, copper losses, excitation losses, and iron losses. In what follows, we are going to detail each one of these components [9].

A. Mechanical losses

These losses can be estimated by empirical formulations, but are generally obtained by the measurement. The approximate law used for modeling the behavior of these losses versus speed, [10], is expressed as follows:

$$P_m = P_v + P_f = 8D\ L_r + 0{,}15\ v^2 \tag{5}$$

B. Copper losses

The stator is equipped by a three-phase armature winding in which copper losses correspond to $R_s I_s^2$ losses and stray load losses as a result of skin effect and proximity effect which make R_s depend on temperature variation. This can be calculated as:

$$P_{jstator} = 3R_s\ T\ I_s^2 \tag{6}$$

With:

$$R_s\ T\ = \rho_s\ T\ \frac{L_{spiremoy} N_{Spires}}{S_{filstator}} \frac{1}{a}\left(\frac{1}{3}\right)^{\delta} \tag{7}$$

C. Excitation losses

These losses are analytically expressed as follows:

$$P_{ex} = R_f I_f^2 \tag{8}$$

D. Iron losses

According to the conventional model of Bertotti, the iron losses of a magnetic material can be divided into three categories [10], [11]: the hysteresis losses caused by magnetic hysteresis of the material when a varying magnetic field is applied to the magnetic material, the eddy current losses resulting from circulating induced eddy currents and the anomalous losses known as the most complex losses phenomena in the magnetic material. It is related to a change in the domain walls of the material.

The iron losses have a considerable influence on the efficiency, particularly at high speed frequency. In this work, we adopt an analytical model with reasonably accurate and short calculation time to be associated with gradient constrained optimization process. For a sinusoidal magnetic flux density, equation (9) was proposed in [11] to predict these losses. Then, some improvements have

been made taking into account the non-sinusoidal periodic regime. The generalized formulation is given by equation (10).

$$P_{fer} = P_{hyst} + P_{cf} = K_h f B_m^{\alpha} \mid K_{cf} f^2 B_m^2 \tag{9}$$

$$P_{fer} = K_h f B_m^{\alpha} + \frac{K_{cf}}{2\pi^2}\left(\frac{dB}{dt}\right)^2 \tag{10}$$

$$\text{with}\left(\frac{dB}{dt}\right) = \sqrt{\frac{1}{T}\int_0^T \left(\frac{dB}{dt}\right)^2 dt} \tag{11}$$

In the case of the HE2A, stator and rotor profiles are given in Fig.3. Iron losses in this alternator are composed of two parts: the stator iron loss and the rotor iron one.

❖ The stator iron losses

✓ Iron losses in the teeth

The evolution of magnetic induction at no-load operation in the teeth is trapezoidal. When the tooth is placed in the inter-polar space, the crossing induction is assumed to be zero. Besides, it increases linearly to reach the maximum under each pole. However, under load, the evolution of the teeth induction is no longer trapezoidal due to the armature reaction and the appearance of space harmonics.

In the present work, space harmonics are not considered and the teeth iron losses could be expressed, [11], as:

$$P_{fer\_dents} = K_{hf} f B_{dm}^{\alpha} + K_{cf}\frac{4mq}{\pi^2} f^2 B_{dm}^2 \tag{12}$$

✓ Iron losses in the cylinder head

The stator magnetic circuit includes two parts. The first is the usual laminated cylinder composed of iron sheets aimed to the insertion of alternator armature. Although, the second part is a massive cylinder surrounding the laminated part intended for flux's flowing and called "stator yoke", [5].

The iron losses in laminated and massive cylinders are respectively expressed by equations (13) and (14).

$$P_{cu\_iam} = K_{hi} f B_{cui\_m}^{\alpha} + K_{ci} f^2 B_{cui\_m}^2 \tag{13}$$

$$P_{cu\_mass} = K_{hm} f B_{cm\_m}^{\alpha} + K_{cm} f^2 B_{cm\_m}^2 \tag{14}$$

✓ Iron losses in the magnetic collector

Built HE2A prototype includes two magnetic collectors on both sides of the yoke (XC10 steel). The iron losses in these collectors are calculated as in the case of the massive cylinder. Assuming that the evolution of induction is sinusoidal, we can write:

$$P_{collector} = K_{hm} f B_{co\_m}^{\alpha} + K_{cm} f^2 B_{co\_m}^2 \tag{15}$$

❖ The rotor iron losses

The analysis and calculation of iron losses in the rotor side are more complex due to the special massive rotor structure gathered magnets inserted in-between adjacent claws. These most significant part of these losses are ones due to eddy currents. However, iron losses in permanent magnet represent an insignificant fraction that is why they are neglected in this work.

The iron losses in the claw pole alternator can be divided into two parts:

✓ No-load iron losses

The variation of the air gap permeance as a result of stator slots allows creating local induction variations on the surface of rotor poles. This variation creates an induction armature current phenomenon that it causes losses. These iron losses are expressed in [9] by:

$$P_s = K_s \left(K_c - 1\right)^2 B_e^2 v^{\frac{3}{2}} pas_{dentaire}^{-\frac{1}{2}} b \tag{16}$$

✓ Load iron losses

The stator winding generates a discontinuous distributed f.m.m in the air gap due to finite number of slots. Thus, enclosed harmonics produce losses at claws surface. Referring to [10], [11], the load iron losses are given by equations (17):

$$P_s = K_s \left(\Delta B\right)^2 v^{\frac{3}{2}} pas_{dentaire}^{\frac{1}{2}} \tag{17}$$

Where: ΔB is the amplitude of a sinusoidal induction given by equation (24) and A_u is the useful line load.

$$\Delta B = \mu_0 A_u \sqrt{2}\frac{pas_{dentaire} - b}{4e_1} \tag{18}$$

D. Losses in DC bridge

These losses are caused by forward voltage drop (V_{diode})and depend essentially on the threshold voltage (V_d), the resistance of the diode in conducting states (R_d) and the diode current (I_d). Then, losses in a diode are expressed by:

$$P_d(t) = V_{diode}(t) i(t) = \left(R_d i_d(t) - V_d\right) i(t) \tag{19}$$

With: $i(t) = I_s\sqrt{2}\sin(\omega t)$ (20)

Referring to [9], the total losses in diodes of a bridge are given by the following formula:

$$P_d = 6 I_S\left(\frac{v_d\sqrt{2}}{\pi} + \frac{R_d I_S}{2}\right) \tag{21}$$

E. Simulations results

Based on the previous analysis, we provide in Fig. 5 and Fig. 6 an analytical visualization of various losses inside of the HE2A versus training speed while the alternator debates 300W and 600W, respectively.

These losses are determined using the alternator reluctance network of Fig. 4.

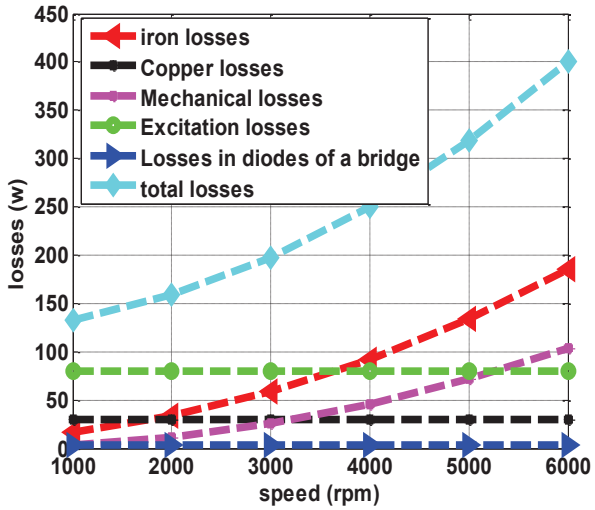

Fig. 5. Calculated alternator losses at 300W.

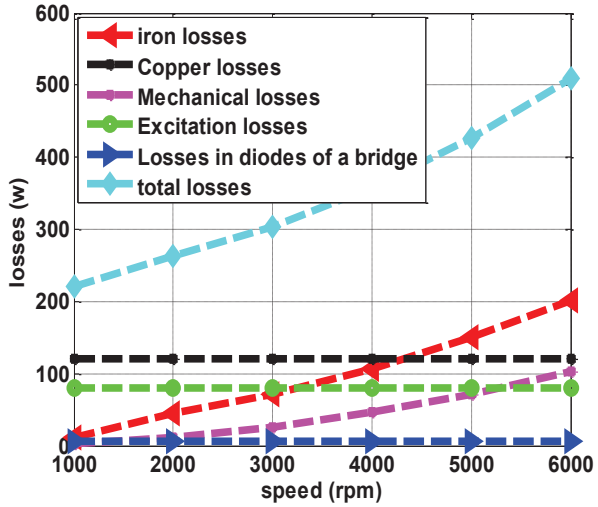

Fig. 6. Calculated alternator losses at 600W.

Furthermore, Fig. 7 illustrates the total loss versus field current for two speeds (1000 rpm and 4000 rpm). The increase in losses is clearly related to the field current and the training speed ones.

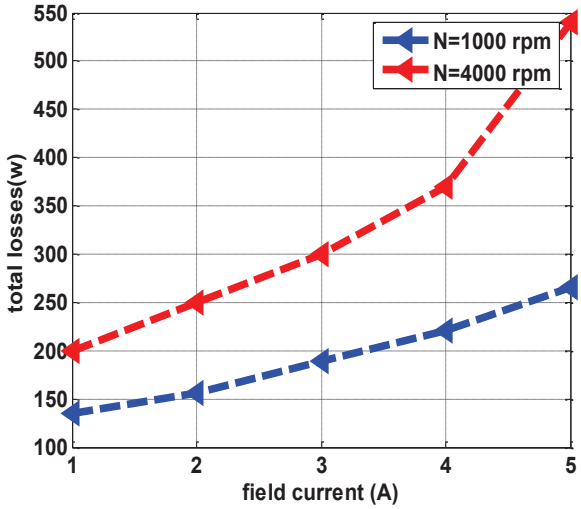

Fig. 7. Calculated load total losses versus field current.

As an outcome of the previous study, the efficiency of the hybrid alternator is evaluated based on equation (22) and illustrated considering the following cases:

- Case 1: for a fixed load power of 600W, Fig. 8 shows the efficiency of the HE2A versus the field current, for two different training speeds: 1000 rpm (law speed) and 4000 rpm (high speed).
- Case 2: for a varied output power (300W then 600W), Fig. 9 illustrates the efficiency of the HE2A versus the training speed.

$$\eta = \frac{P_u}{P_u + \sum losses} \tag{22}$$

Analyzing obtained curves one can notice that:

- For a fixed value of the excitation current and a constant output power, the efficiency of the alternator decreases when the training speed increases, Fig 8 and Fig.9.
- For a constant speed training speed, the variation of the output power has no significant effect on the alternator efficiency, Fig.9.

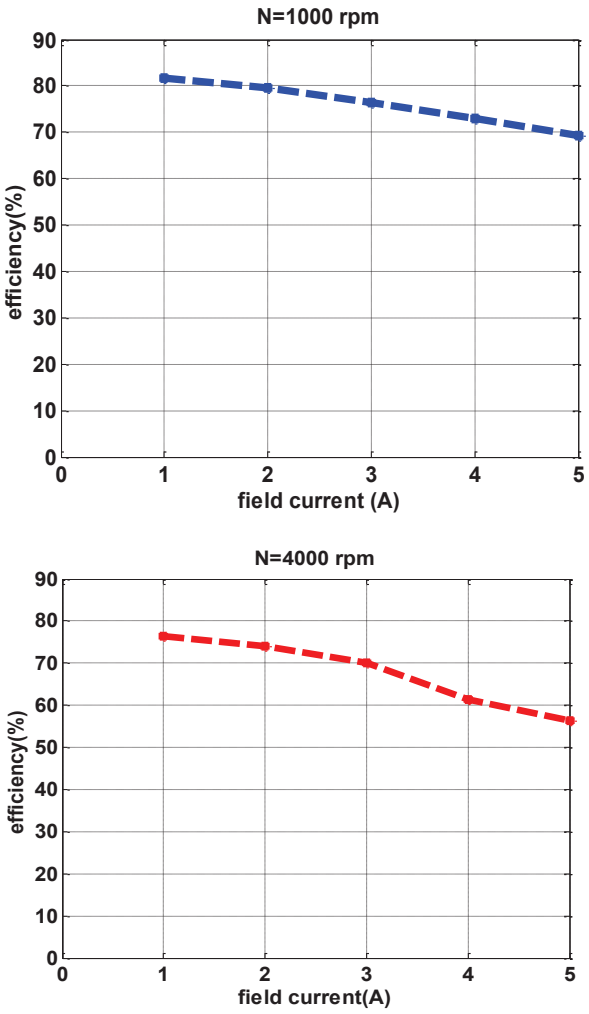

Fig. 8. HE2A efficiency versus field current

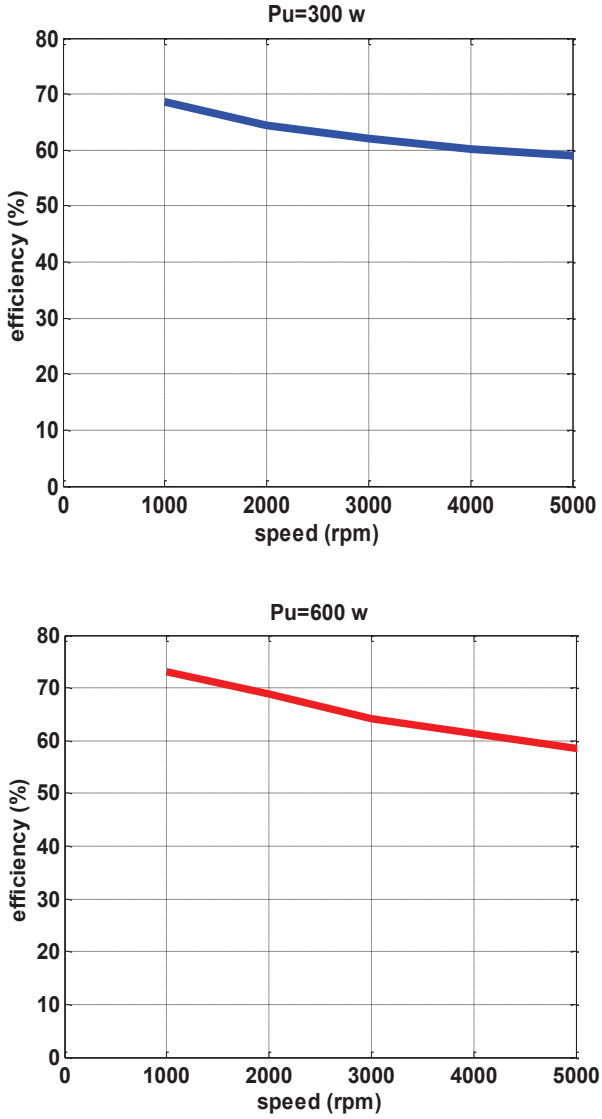

Fig. 9. HE2A efficiency versus speed.

4. Optimization of the HE2A with Minimized Iron Losses

A. Presentation of the problem

A well-defined MEC is an interesting mean for optimization, due to its accuracy and low computation time. Considering previous studies, we can conclude that the particular rotor structure of the HE2A leads to high iron losses rates, especially when training speed increases. Consequently, in the present section we are going to optimize the alternator topology considering iron losses minimization case.

To do so, proposed magnetic equivalent circuit is coupled to an optimization procedure, based on Sequential Quadratic Programming (SQP) and developed on MATALB Software platform, as shown in the synopsis of Fig. 10. Calculations was performed for two operating points of the alternator (1000rpm and 4000rpm) corresponding respectively to a law speed operation point and high speed operation point.

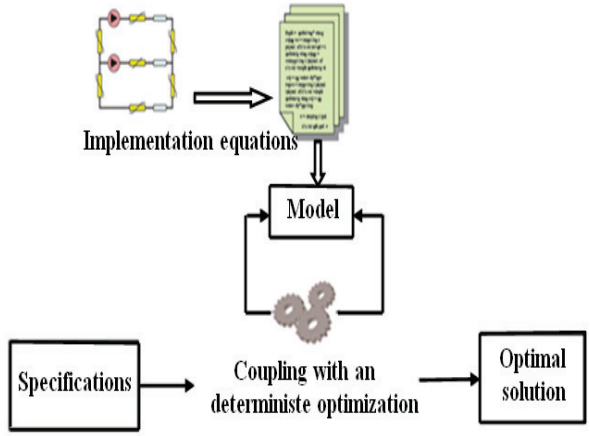

Fig. 10. Generation of the optimization algorithm.

B. Optimization variables

The transition from a simple excited to a hybrid excited alternator where field winding is transferred from rotor to stator side leads us to analyze the areas of variation of specific geometric variables that can have a considerable impact on the HE2A performance. In the present work, four geometrical parameters are chosen to perform optimization with minimized iron losses: the magnetic collector thickness e_{cm} , the outer yoke thickness h_{c1} , the active length of the stator yoke l_{stator} and the massive cylinder length l_{c1} . These parameters are illustrated in Fig. 11 and their variation limits are summarized in Table I. It is to be noted that outer dimensions of the original prototype are kept constant during the optimization process.

Fig. 11. The input parameters to optimize.

TABLE I

Constraints imposed on the geometric parameters

Geometry parameters	Designations	min (mm)	max (mm)
e_{cm}	magnetic collector thickness	4	10
h_{c1}	outer yoke thickness	2	7
l_{stator}	active length of the stator yoke	28	32
l_{c1}	massive cylinder length	25.1	27.1

C. Output performance optimization

Table II gives kept values of the optimization variables provided by computing procedure. Following these values,

the HE2A iron losses and efficiency are calculated then illustrated in Fig. 12 and Fig. 13.

Analyzing these figures, one can notice that:

- At 1000rpm, iron losses decrease from 12.6W to 9.46W, and the efficiency grows from 73.05% to 73.36% (Fig. 12). Thus, we can conclude that, at low speed, the efficiency gain is of little importance because iron losses reduction is not consequent.
- At 4000rpm, iron losses are reduced from 109W to 72.06W and the efficiency jumps from 62.3% to 65% (Fig. 13). Consequently, the decrease of iron losses and the improved of the efficiency is more important at high speed.

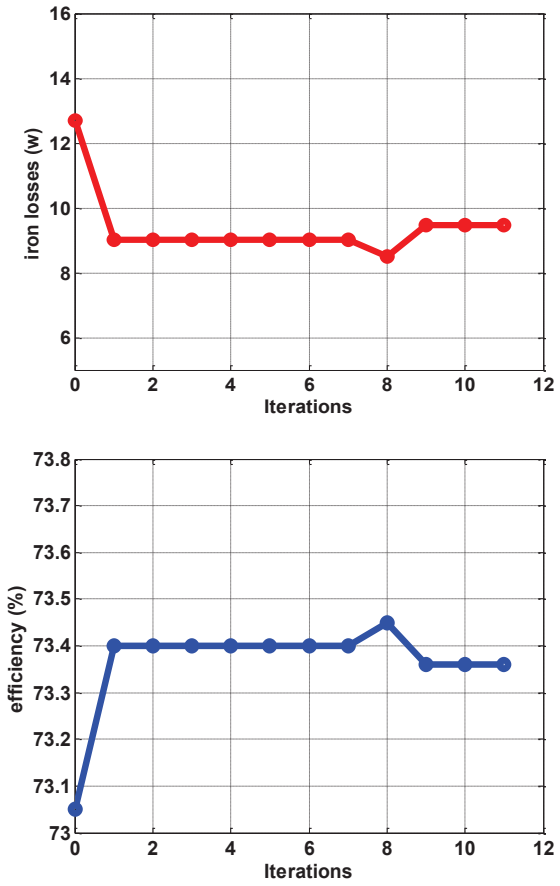

Fig. 12. Evolution of iron losses and efficiency during optimization at 1000rpm.

TABLE II

Evolution of optimization parameters

Geometry parameters	initial value (mm)	optimal value (mm)
e_{cm}	6.1	4
h_{c1}	5	7
l_{stator}	31	32
l_{c1}	25.63	25.1

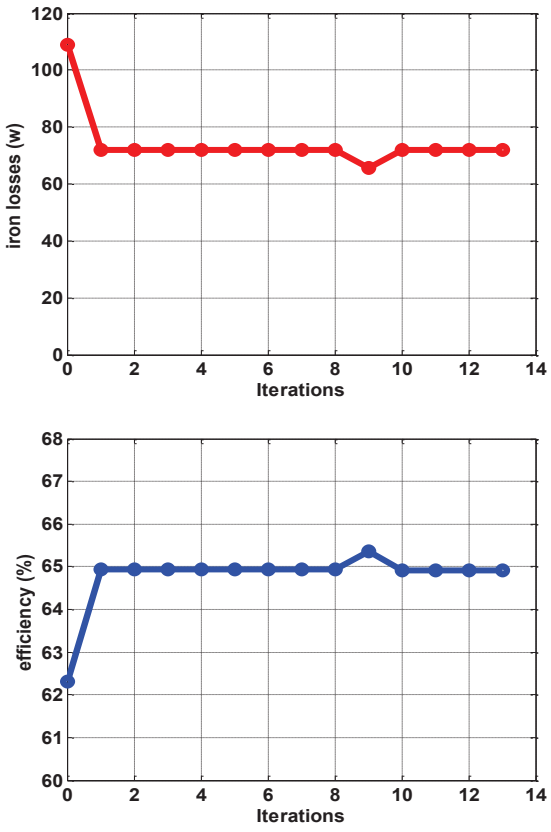

Fig. 13. Evolution of iron losses and efficiency during optimization at 4000rpm.

4. Conclusion

In a previous work [5], beneficial effect of the hybridization of excitation sources has been confirmed on a claw pole alternator's generation capabilities. Indeed, performed study was based on a magnetic equivalent circuit models validated experimentally. It has been found that the HE2A presents higher performances, due to the increase of leakage flux through the integration of Barium ferrites permanent magnets between adjacent rotor claws. However, the transfer of field winding from rotor side to stator one leads to the increase of massive parts of the alternator magnetic circuit. The present work can be qualified as a compliment study aimed to the optimization of the alternator topology while outer dimensions are kept constant. Proposed process is based on a SQP program coupled to the MEC model of the HE2A targeting the minimization of iron losses. Obtained results prove that the decrease of these losses is more important at high speed which leads to a higher improvement of the alternator efficiency.

References

[1] L. Tutelea, D. Ursu, I. Boldea, and S. Agarlita,"IPM claw-pole alternator system for more vehicle braking energy recuperation," *Journal of Electrical Engineering*, pp. 1-10, 2013.

[2] J. Sohn, S. Hong and M. Sunwoo, "Alternator Torque Model Based on Equivalent Circuit of Synchronous Generator for Electric Power Management," *IEEE transactions on vehicular technology*, vol. 62, no. 8, october 2013.

[3] S.C. Tang, D.M. Otten, T.A. Keim, and D.J. Perreault, "Design and Evaluation of a 42 V Automotive Alternator with Integrated Switched-Mode Rectifier," *IEEE Transactions on Energy Conversion*, Vol. 25, No. 4, pp. 983-992, Dec. 2010.

[4] H. Aloui, A. Ibala, A. Masmoudi, M. Gabsi and M. Lecrivain, " *Reluctant network based investigation of a claw pole alternator with dc excitation in the stator*", in Inter. Journal for Computation and Mathematics in Electrical and Electronic Engineering, vol. 27, no. 5, pp.1016-1032, 2008.

[5] M. Klach, H. Aloui, R. Neji, M. Gabsi and M. Lecrivain, "Hybridization effect on generation capability of an embedded CPA, " *Journal of Electrical Systems*, pp 133-145, Vol. 12, No. 1, 2016.

[6] V. Ostovic, J. M. Miller, V. K. Garg, "A Magnetic Equivalent-Circuit-Based Performance Computation of a Lundell Alternator," *IEEE Transactions on Industry Applications*, Vol. 35, no. 4, july/august 1999.

[7] Sasareka M. Gunawardana; Philip A. Commins; Jeffrey W. Moscrop; Sarath Perera, Applicability of nonlinear reluctance model to a closed core Fault Current Limiter, PowerTech, 2015 IEEE Eindhoven, pp: 1 – 6.

[8] A.Delale, L.Albert, L.Gerbaud, and F.Wurtz, "Automatic Generation of Sizing Models for the Optimization of Electromagnetic Devices Using Reluctance Networks," *IEEE Trans .Magn*, vol. 40, no. 2, March 2004.

[9] B. Ganji, Z. Mansourkiaee, J. Faiz, A fast general core loss model for switched reluctance machine, *Original Research Article, Energy, Volume 89, September 2015, Pages 100-105*

[10] A. Ammar, " Modélisation et Optimisation d'un Générateur Synchrone à Double Excitation de Forte Puissance" PhD. Dissertation, University of Lille North of France,2013.

[11] L. Albert, Modelling and optimization of claw pole alternators applied to automotive systems (in French), PhD Dissertation, *Institut National Polytechnique de Grenoble*, France, 2004.